Appl. Phys. A 58, 523–534 (1994)

Applied Physics A Solids and Surfaces

Elastic Modulus and In-Plane Thermal Diffusivity Measurements in Thin Polyimide Films Using Symmetry-Selective Real-Time Impulsive Stimulated Thermal Scattering

J. A. Rogers, Y. Yang, K. A. Nelson

Department of Chemistry, Massachusetts Institute of Technology, Cambridge, MA 02139, USA

Received 18 June 1993/Accepted 16 November 1993

Abstract. We describe a technique for extending the utility of the real-time Impulsive Stimulated Thermal Scattering (ISTS) method for thin film characterization. Using weakly absorbed excitation pulses, we show how to selectively drive acoustic waveguide modes that are unobservable when strongly absorbed pulses are used. The ability to excite and monitor these modes is important because it allows for a significant increase in the experimental sensitivity to the film longitudinal velocity. This arrangement also greatly simplifies determination of the in-plane thermal diffusivity. The technique is illustrated through study of unsupported polyimide films with six different thicknesses.

PACS: 43.35.Pt, 44.90+f, 68.60.Bs, 68.60.Dv, 78.47.+p

Polymer films find ever increasing use in device applications in the microelectronics, aerospace, and biomedical industries. Characteristics of importance include the mechanical moduli, the degree of adhesion, and the thermal diffusivity. Recently we showed how to determine these properties in unsupported and silicon-supported polyimide films with a novel characterization technique that is noncontact, nondestructive, has real-time ($\approx$ms) data acquisition rates, and high ($\approx$50 μm) spatial resolution [1, 2]. The method involves optical excitation and detection of acoustic waveguide modes and thermal disturbances and is based on transient grating methods used in the past [3, 4]. The information obtainable from such experiments can be used to determine the elastic and loss moduli as well as the degree of adhesion and the thermal diffusivity.

Although we were able to accurately characterize the mechanical properties in supported and unsupported films, in the unsupported films the accuracy of the fitted longitudinal velocity was limited due to the nature of the acoustic disturbances that were excited. Here we show that by selectively exciting modes that are sensitive to the longitudinal velocity of the film, we are able to significantly increase the experimental sensitivity to this parameter. To achieve this selective excitation, we employ different excitation wavelengths, a method first discussed and demonstrated in anthracene flakes by Meth et al. [5]. In particular, we use wavelengths which are only weakly absorbed by the film. By using both strongly and weakly absorbed excitation wavelengths, the effort required to accurately determine the film moduli is reduced.

The in-plane thermal diffusivity can also be determined with this arrangement. We believe that this method has certain advantages relative to other existing noncontact methods for thermal diffusivity evaluation when applied to systems with high surface to volume ratios and low diffusivities. One reason for this is that in such cases, the thermal properties of the surroundings are nonnegligible in most experimental arrangements [6, 7]. Accounting for heat flow into the surrounding fluid complicates analysis and often frustrates accurate determination of the film thermal properties [8]. With the experimental arrangement described here, we can determine the in-plane thermal diffusivity without complications due to thermal transport through the thickness of the film, or from the film to the air. Our technique thus complements the two most commonly used techniques for thin polymer film thermal characterization, the flash method [9] and the thermal wave method [10], both of which are sensitive only to the out-of-plane thermal diffusivity. We note that an experimental geometry similar to ours but using strongly absorbing excitation pulses and a different probing method has been used to determine thermal diffusivities in thin superconducting films [6]. In this case, with precise knowledge of the film absorptivity at the exciting and probing wavelengths, a computationally intense yet tractable analysis allows for extraction of anisotropic thermal diffusivities.

The method described in this paper represents a simple yet powerful extension of the real-time Impulsive Stimulated Thermal Scattering (ISTS) technique for thin film characterization [1, 2]. In ISTS, two picosecond pulses are temporally and spatially crossed in an absorbing sample. Interference of these pulses creates a grating intensity pattern which induces impulsive heating in the film with the same grating geometry. Thermal expansion following this

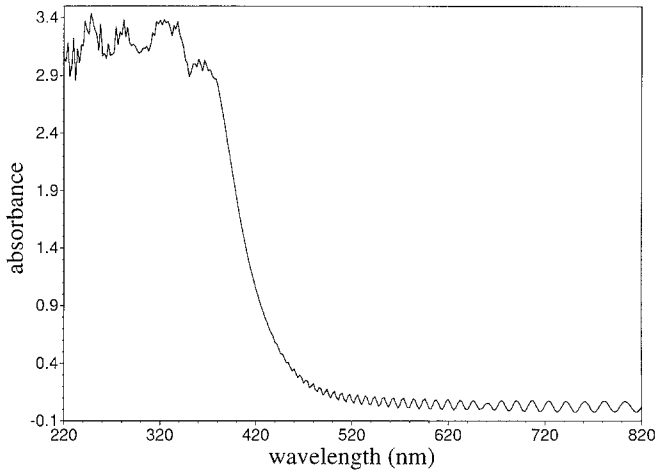

Fig. 1. UV-VIS absorption spectrum of an 8.46 μm unsupported PI2555 polyimide film Excitation pulses used in the past (266 nm and 355 nm) are strongly absorbing compared to those used in this study (532 nm)

deposition of heat drives acoustic and thermal responses with well-defined (grating) wavevectors. Diffraction of a cw probe beam from the resulting material grating is used to determine the temporal evolution of the material motions. In previous work, 266 nm or 355 nm pulses were used for excitation of polyimide films. As shown by the absorption spectrum in Fig. 1, both of these wavelengths are strongly absorbed by the films. In this report we show that weakly absorbed (532 nm) excitation pulses permit selective excitation of acoustic waveguide modes that are spatially symmetric and which were unobservable with 266 nm excitation using the same experimental arrangement. In addition, off-resonant excitation deposits heat uniformly through the film thickness, minimizing effects of out-of-plane heat flow and thereby allowing for very straightforward determination of the in-plane thermal diffusivity.

The paper is organized as follows. First, we briefly describe the ISTS technique and experimental arrangement. We then show typical data collected with the modified experimental apparatus. The idea for symmetry-selective excitation is qualitatively described, and procedures for acoustic and thermal data analysis are outlined. Using these procedures we determine best fit values for the intrinsic longitudinal and transverse velocities for six polyimide thin films based on data presented here and data presented previously [2]. In addition, we describe the advantages of using off-resonant excitation for in-plane thermal characterization and use this method to determine the thermal diffusivity for each of the six samples. Finally, and perhaps most importantly, we demonstrate the feasibility of complete mechanical and thermal film characterization in a single laser shot.

1 Experimental Apparatus and Typical Data Scans

The experimental arrangement used here is very similar to that described previously [1, 2] (see Fig. 2). The excitation pulse is derived from the output of a Q-switched, modelocked, and cavity dumped Nd : YAG laser which yields a 1 mJ, 1064 nm pulse of 100 ps duration at a repetition rate of up to 1 kHz. This output is passed through a Lithium triBOrate (LBO) crystal to yield light at 532 nm. These pulses are attenuated and passed through a 50% beam splitter. The two resulting beams are crossed at an angle θ and the relative path lengths and mirror positions

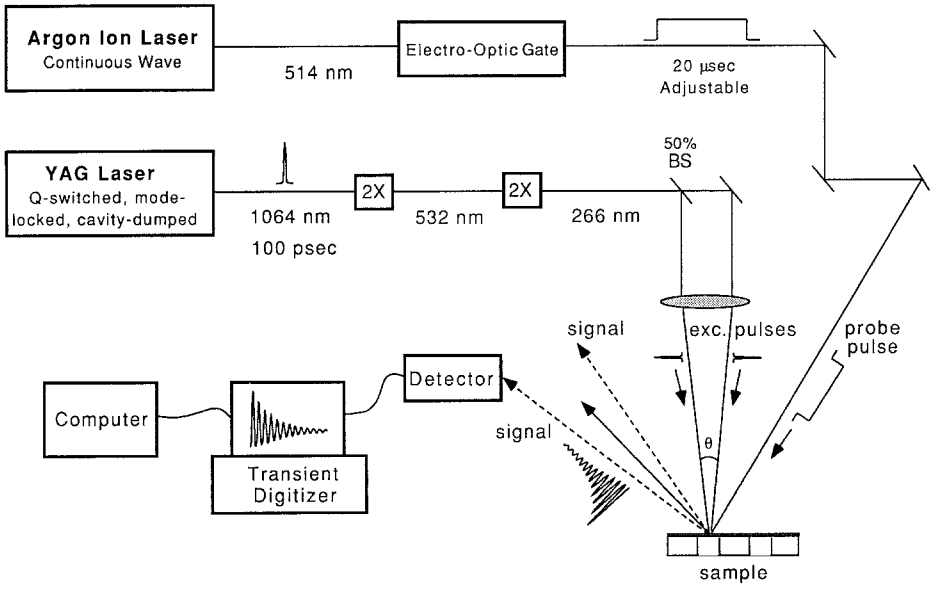

Fig. 2. Experimental setup for real-time ISTS experiments on thin films using weakly absorbed excitation pulses. Two picosecond excitation pulses at 532 nm are crossed at the sample surface. Motions induced by the excitation pulses are monitored with a probe derived from an electro-optically gated cw laser which is spatially and temporally overlapped with the excitation beams at the sample. The diffracted signal is time resolved electronically with a fast photomultiplier tube and a transient digitizer. The diffracted signal can be collected in reflection mode as shown here, or in transmission mode. BS: beamsplitter; 2X: second-harmonic generator

are adjusted such that the pulses are temporally and spatially coincident at the film surface. Interference between the two excitation pulses gives rise to a grating intensity pattern with a wavevector of magnitude

$$q = \frac{4\pi \sin(\theta/2)}{\lambda_1} = \frac{2\pi}{\Lambda}, \quad (1)$$

where λ_1 is the laser wavelength, θ is the angle between the excitation pulses, and Λ is the grating fringe spacing. Table 1 lists the crossing angles and corresponding grating wavelengths used in this set of experiments. Although it is possible to use a calibrated mechanical rotation stage to determine the wavelength of the grating through (1), we found that more accurate results could be obtained by burning a grating into a blank silicon wafer. The wavelength of this burn mark was determined to within 0.05 μm using a standard optical microscope.

The material response induced by the crossed excitation pulses was determined in real-time by monitoring the time-dependent diffraction of a probe pulse that is overlapped with the excitation pulses. A continuous wave (cw) single-mode argon-ion laser (Lexel 3500) which produces 1 W at 514 nm with a flat intensity profile was used. This output is electro-optically gated (Conoptics 380) to yield a square pulse whose temporal width is adjustable from ≈500 ns to many seconds. A fast photomultiplier tube (Hamamatsu 1P28) and a digitizing oscilloscope (Tektronics DSA 602) were used to temporally resolve the diffracted intensity.

Table 1. Summary of angles and corresponding grating wavelengths used for experiments described in the text

Excitation angle (θ) in degrees ($\pm 0.05°$)	Grating wavelength (Λ) in μm (± 0.05 μm)
0.66	55.80
0.74	46.18
1.01	29.70
1.27	24.10
1.28	21.35
1.56	18.24
1.75	18.02
1.93	16.19
2.07	14.20
2.20	13.36
2.47	13.00
2.55	11.85
2.72	11.63
2.98	10.26
3.08	9.85
3.30	8.98
3.63	8.39
3.74	8.33
4.08	7.45
4.45	6.96
4.73	6.60
4.88	6.29
4.93	6.26
5.47	5.43
6.10	4.99
6.76	4.52
7.15	4.25
7.92	3.90
8.92	3.43
9.03	3.36

This experimental arrangement was used to characterize free standing polyimide films. Sample fabrication has been discussed previously [2, 12–15]. Briefly, the samples were produced by spin coating and fully curing Dupont PI2555 (BTDA/ODA/MPD) on 10 cm diameter silicon wafers. By etching the silicon in two selected regions with an acid mixture (a 6 : 1 : 1 mixture of $HF : HNO_3 : CH_3COOH$), free standing regions of film were prepared. The thicknesses of the six samples determined prior to etch were 1.56, 2.16, 3.18, 4.40, and 8.46 ± 0.05 μm. For experimental convenience we monitored diffracted light appearing in transmission mode. We also collected reflection mode data at two angles to verify that symmetry selective excitation is also useful when measurements are made in this geometry.

Although it is possible to collect data in one laser shot, all data used for analysis were the result of the average of 200 single laser shot data scans and required approximately 2 s to collect. Typical 200 averaged data are presented in Fig. 3. The upper frame of this figure shows acoustic oscillations induced with weakly absorbed green (532 nm) excitation pulses in the 8.46 μm film with a grating wavelength of 55.80 μm, along with data with a grating wavelength of 50.67 μm collected using strongly absorbed UV (266 nm) excitation pulses. It is clear that there are dramatic differences between the two data scans. The lower frame of Fig. 3 gives the power spectra of both sets of data and shows that in the case of 266 nm excitation, the material response is dominated by a single low frequency oscillation. In contrast, the response to 532 nm excitation consists of two relatively high frequency acoustic motions. We explain the meaning of these differences and how they arise in the next section. Figure 4A shows decay of the grating signal at longer times when 532 nm excitation pulses are used. Figure 4B gives the log of the diffracted intensity given in Fig. 4A. The linear form of this curve demonstrates that the decay is single exponential. The decay rate is controlled by the excitation wavevector and the thermal diffusivity of the film. From data like those shown in Fig. 3 we determine acoustic mode phase velocities and damping rates which in turn yield elastic and loss moduli. From data like those in Fig. 4 we determine the in-plane thermal diffusivity.

2 Theory

2.1 Acoustic Response

A detailed description of ISTS excitation and probing of acoustic responses in thin unsupported films has been given in [2, 5]. Briefly, because typical wavelengths of acoustic disturbances excited with ISTS are of the same order as the thickness of films used in these experiments, strong waveguide effects are observed. For every acoustic wavevector (q) times thickness (d) value, a number of distinct acoustic modes, known as Lamb modes, can propagate. The dispersion of these modes for a typical polymer film is given in Fig. 5. Each line in this figure corresponds to a different waveguide (Lamb) mode. The displacement fields

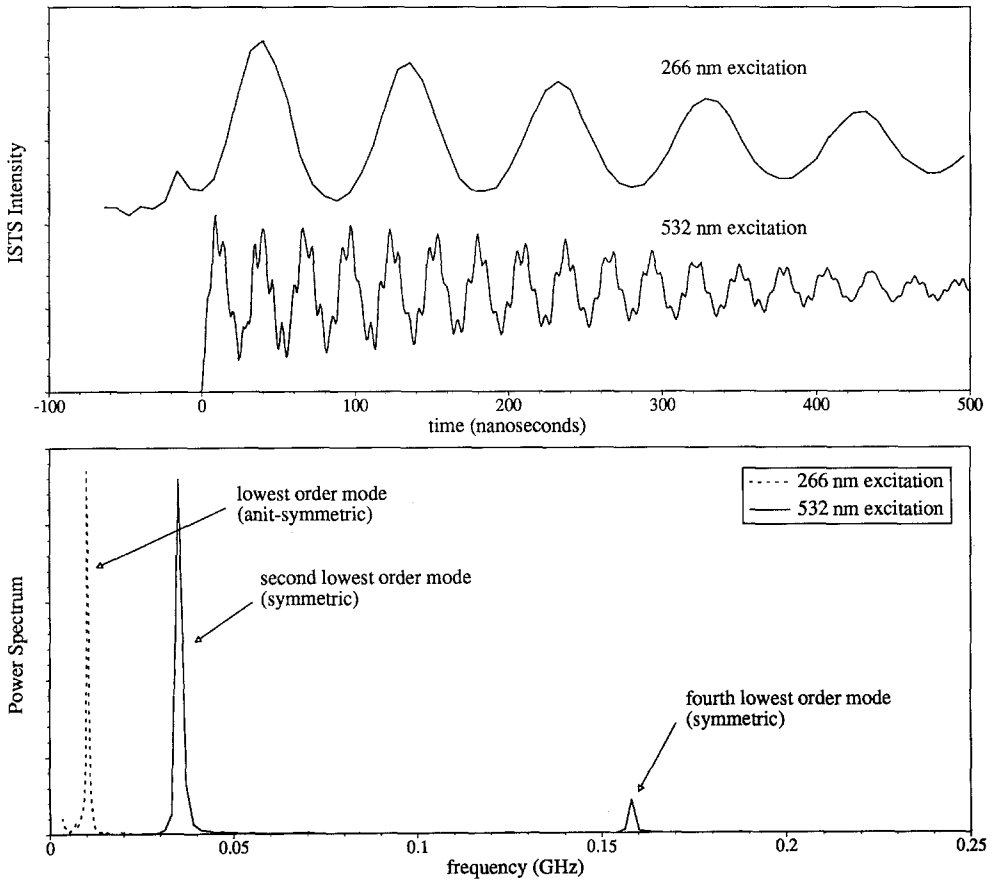

Fig. 3. ISTS signal from an 8.46 μm unsupported PI2555 polyimide film using strongly absorbed 266 nm and weakly absorbed 532 nm excitation pulses at acoustic wavelengths of 50.67 μm and 55.80 μm, respectively, are displayed in the *upper frame*. Both of these data scans are the result of 200 averages. Dramatic differences are a result of different symmetry properties of the thermal driving forces derived from the different colored excitation pulses. The power spectrum given in the *lower frame* shows that a slow monochromatic material motion is induced by strongly absorbed excitation while weakly absorbed excitation pulses excite two relatively high frequency motions

of the four lowest-order Lamb modes at a qd value of 2.5 are illustrated in Fig. 6. With strongly absorbing excitation pulses and a off-resonant probe, primarily the lowest-order Lamb mode is excited and monitored in reflection mode (see Fig. 3). Detailed analysis of the excitation and probing mechanisms explained why this is the case. Qualitatively, excitation pulses that are absorbed strongly most efficiently drive modes with large displacements at the surfaces of the film. In addition, the largest displacements are induced in modes with small phase velocities and hence small effective stiffnesses. Further, in reflection mode the diffraction of probe light is primarily due to surface ripple, and is therefore most sensitive to those modes which involve large surface corrugation. Since the lowest-order Lamb mode satisfies all of these conditions, it dominates the data at nearly all acoustic wavelengths. As indicated in Fig. 6, this mode has largely transverse (shear) character. As a result, the magnitude and dispersion of the lowest-order mode phase velocity is more sensitive to the transverse velocity (and shear modulus) of the film than to the longitudinal velocity (and bulk modulus). This is reflected in the magnitude of the uncertainties for the longitudinal velocities that we determined previously [2]. In fact, with UV excitation we showed that it was necessary to map out a significant portion of the dispersive region of the lowest-order mode in order to determine the longitudinal velocity to any reasonable degree of accuracy. This difficulty can be circumvented by selectively exciting modes that are more sensitive to the longitudinal velocity. Weakly absorbed excitation pulses can be used to achieve this goal [2, 5]. Pulses that are weakly absorbed generate a thermal distribution that is symmetric with respect to the plane passing through the center of the film and parallel to the film surfaces. Because of this, only modes with the same symmetry (i.e. symmetric Lamb modes) will be excited. Since the magnitude and dispersion of the second lowest-order Lamb mode is sensitive to the longitudinal velocity, and since this mode is the lowest symmetric mode, experimental sensitivity to the longitudinal velocity is increased with off-resonant excitation. As a result, with a combination of resonant and off-resonant excitation, we can obtain film properties with a higher degree of accuracy and at the same time reduce the number of excitation angles needed to do so. This is demonstrated in Sect. 4.

Since the utility of using symmetry-selective excitation hinges on the ability to excite and probe other than the lowest-order Lamb mode, we briefly describe a peculiar feature of the excitation efficiency of the second lowest

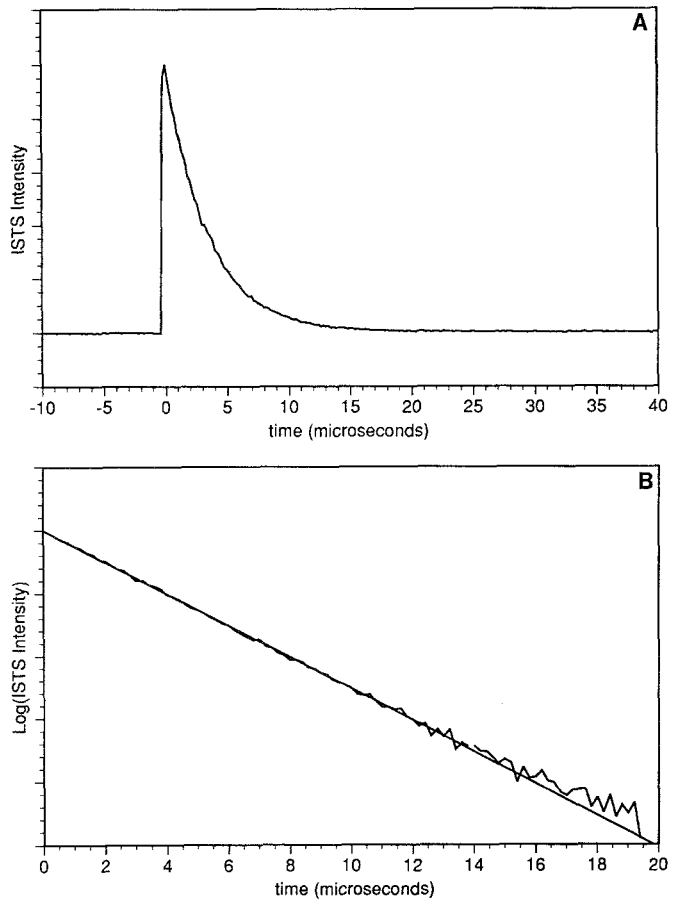

Fig. 4A, B. ISTS data on a microsecond time scale from an unsupported 8.46 μm PI2555 polyimide film at an excitation wavevector of 0.90 μm^{-1}. These data are the result of 200 averages. **A** shows the decay of the diffracted intensity as a function of time, while **B** shows the time dependence of the logarithm of this intensity. **B** shows that the decay of the diffracted intensity is single exponential. The decay rate and the excitation grating wavelength define the in-plane thermal diffusivity

mode. This mode is particularly important because we tend to excite it preferentially with weakly absorbed excitation pulses. This is because it has a smaller effective stiffness than the other symmetric modes (i.e. it has the lowest velocity) and because at most experimentally accessible values of qd, its strain distribution closely matches that induced by off-resonant excitation pulses. In spite of this, it turns out that the excitation efficiency of this mode becomes zero when $qd = \pi$. This is illustrated in Fig. 7 where the maximum displacement induced in the second lowest-order mode by 532 nm ISTS excitation of a 5.29 μm film is plotted against the product of the film thickness and the excitation wavevector. At $qd = \pi$, it is impossible to excite the second lowest-order mode with ISTS. This is a general result as it does not depend on the excitation light absorption length or on film material parameters provided that the film is isotropic.

There are two ways to explain the vanishing excitation efficiency of the second lowest-order mode. One involves an intuitive argument based on the spatial character of the mode. The other is more fundamental and is based on the structure of the equations of thermoelasticity as applied to a thermally driven acoustic slab waveguide. We begin with the intuitive description. At $qd = \pi$, it is easy to show that the phase velocity of the second lowest-order mode is equal to the transverse velocity times the square-root of two. As a result, the transverse and longitudinal displacements take on the following simple forms,

$$u_y \propto \sin(qy)\,, \tag{2}$$

$$u_z \propto \cos(qy)\,, \tag{3}$$

where u_z is the displacement along the surface of the film (or the in-plane displacement), u_y is the displacement perpendicular to the film surface (or the out-of-plane displacement). The y-axis is perpendicular to the film surface and has its origin at the center of the film, and the grating wavevector lies along z. For convenience we have dropped all time dependent factors and proportionality constants. From (2) and (3), we see that at $qd = \pi$, the z displacement is zero at the surfaces of the film and is maximized at the center of the film (see Fig. 7). This spatial structure is wholly incompatible with the ISTS driving force which directly induces motion at the film surface when strongly absorbing pulses are used, and through some significant fraction of the thickness of the film when near or off-resonant pulses are used. In Fig. 7 we also illustrate the displacement character of the second lowest-order mode at values of qd slightly above and slightly below π. While the displacments at these qd values are similar to those at $qd = \pi$, it is evident that for each case, the mode has some depth independent z displacement which allows for coupling to the driving force and results in a finite excitation efficiency. This is in contrast to the situation at $qd = \pi$.

The zero excitation efficiency of the second lowest-order mode can also be explained by appealling to the thermoelastic equations of motion which describe ISTS excitation. Written in terms of displacement potentials and in the absence of body forces, these equations read [16]

$$\nabla^2\phi - \frac{1}{c_1^2}\frac{\partial^2\phi}{\partial t^2} = \frac{\gamma}{\rho c_1^2}T, \tag{4}$$

$$\nabla^2\boldsymbol{\psi} - \frac{1}{c_2^2}\frac{\partial^2\boldsymbol{\psi}}{\partial t^2} = \mathbf{0}\,, \tag{5}$$

with

$$\mathbf{u} = \nabla\phi + \nabla\times\boldsymbol{\psi} \quad \text{with} \quad \nabla\cdot\boldsymbol{\psi} = 0\,. \tag{6}$$

Here $\mathbf{u}$ is the displacement vector, ϕ is the scalar potential, $\boldsymbol{\psi}$ is the vector potential, and T is the temperature. ρ is the density, and c_1 and c_2 are the longitudinal and transverse velocities respectively. γ is a constant related to the elastic Lame constants and the coefficient of linear volume expansion, α_t, by $\gamma = (2\mu + 3\lambda)\alpha_t$.

The thermal distribution set up by the excitation pulses determines the form of T. It is the impulsive creation of this thermal distribution which drives acoustic motions. In the previous work on ISTS of thin films [2], the temperature distribution following excitation was assumed to be temporally static, and (4) and (5) were solved using transform techniques. This resulted in expressions for the potentials in terms of the thermal driving force and four unknown constants associated with the homogeneous solutions. Using the Duhamel-Neumann equation, these constants were determined by requiring the film surfaces

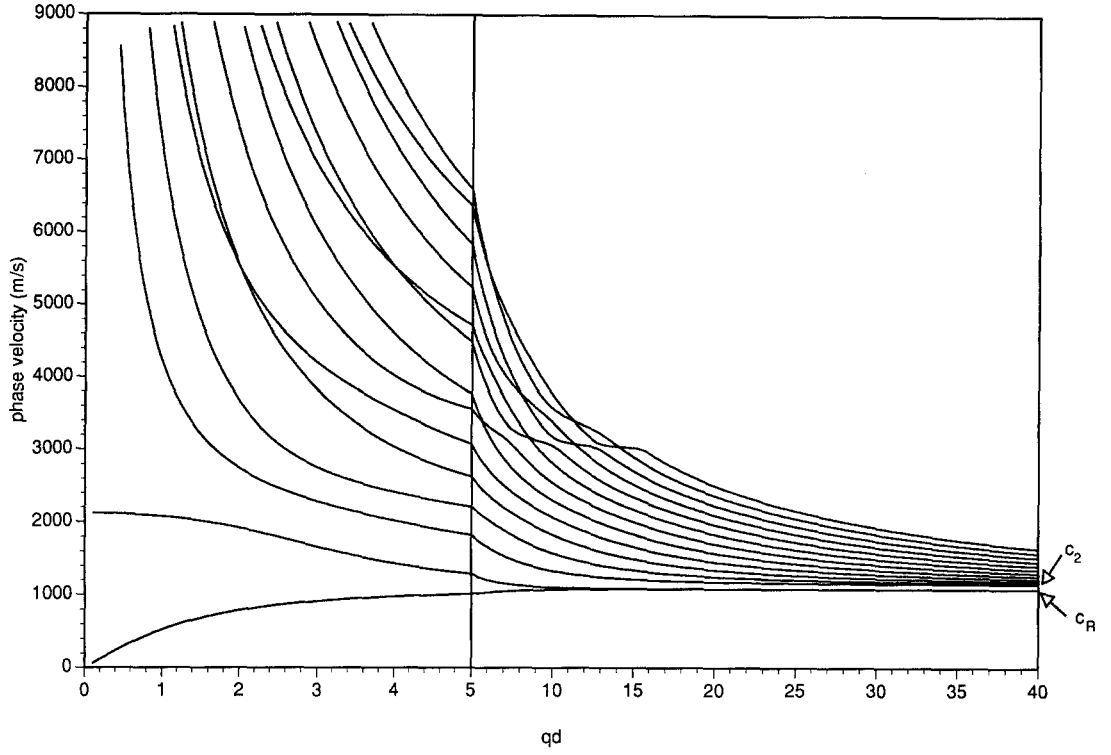

Fig. 5. Lamb mode dispersion curves for a typical polymer film. The film thickness is denoted d, and the acoustic wavevector q. c_2 is the transverse velocity of the film, and c_R is the Rayleigh wave velocity of the film. We have changed the x-axis scale at $qd = 5.0$ to illustrate the asymptotic limits of the curves

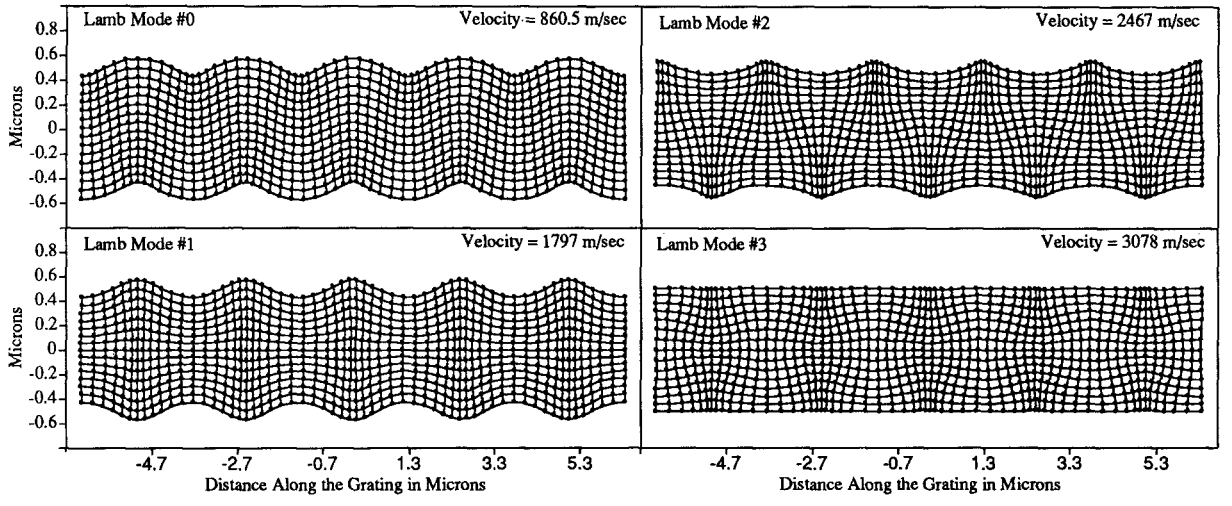

Fig. 6. Lattice distortion diagrams of the lowest four Lamb modes at a wavevector (q) times thickness (d) value of 2.5. The first and third modes are anti-symmetric in displacements along the wavevector direction with respect to the center of the film. The second and fourth modes are symmetric. Strongly absorbed excitation pulses most efficiently drive the lowest-order mode, while weakly absorbed pulses most efficiently drive the second lowest-order mode

to be stress free. The important points are that the ISTS driving force is derived from a temperature increase and that this thermal distribution only directly couples to the scalar potential (4, 5). In general, the vector potential is only needed to match the zero surface stress boundary conditions. In fact, in bulk samples which have no surfaces, the vector potential vanishes, and ISTS only initiates motion in ϕ. It turns out that at $qd = \pi$, the part of the scalar potential associated with the second lowest-order Lamb mode is forced to zero by the zero surface stress boundary conditions. For this reason, the ISTS thermal driving force is unable to directly couple to the scalar potential and is therefore unable to excite the mode.

In closing this section, we note that although this effect has negligible implications on the usefulness of off-resonant excitation, it has noticeable effects on the data in a relatively narrow qd range near π. This is shown experimentally in Sect. 3.1.

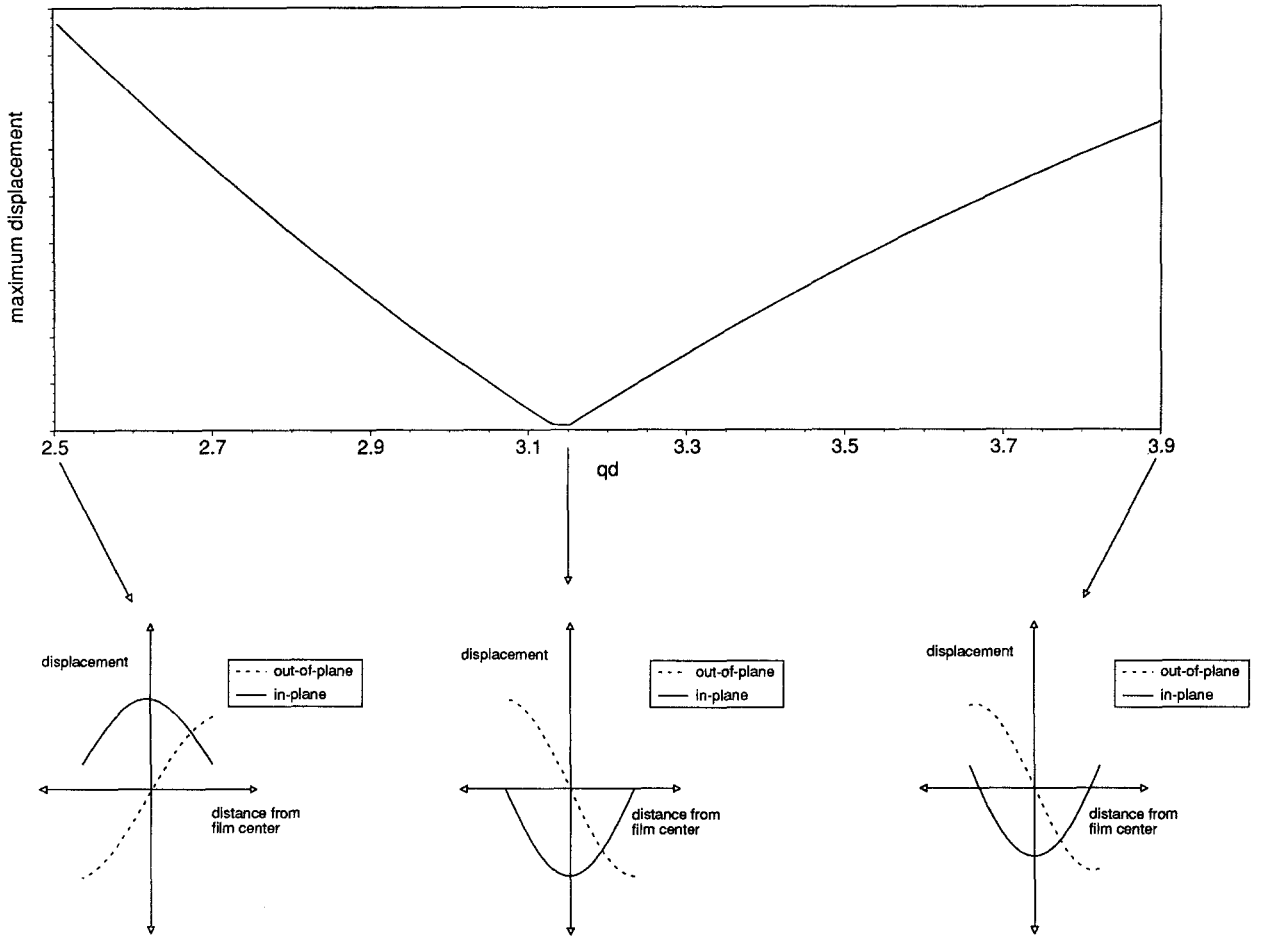

Fig. 7. Maximum displacement amplitude of the second lowest-order mode as a function of wavevector (q) times thickness (d) product induced by 532 nm excitation pulses in a 5.29 μm film. The dip at $qd = \pi$ is a result of the fact that the second lowest-order mode loses all depth-independent longitudinal character in this region. This is illustrated in plots of the depth dependence of the in-plane and out-of-plane displacements in the bottom portion of this figure

2.2 Thermal Response

In ISTS experiments, thermal diffusion rates can be determined from the long-time decay of the diffraction efficiency. When strongly absorbed excitation pulses are used, heating only occurs in a small fraction of the film near the film-air interface. Because of this, thermal diffusion perpendicular to the film plane must in general be considered [8, 11]. Careful incorporation of these effects significantly complicates extraction of material properties, and requires precise knowledge of the film absorptivity at the excitation wavelength. There are, however, several ways to minimize the effects of out-of-plane heat flow. First, it is possible to increase the excitation angle in order to decrease the lifetime of the grating due to diffusion along the length of the film and to thereby decrease the importance of out-of-plane thermal transport whose rate is independent of the wavevector. However, this is in general difficult because the diffraction efficiency (i.e. the surface ripple) is a strongly decreasing function of the excitation wavevector [1, 2]. Another, and more clever way to deal with out-of-plane heat flow is to simply divide two data scans taken at different excitation wavelengths in a point by point fashion [11]. By doing this, the effects of out-of-plane flow are eliminated since its rate is independent of the wavevector. In principle, the result of this division is a curve described by a single exponential decay whose rate is determined by the in-plane thermal diffusivity and the difference of the square of the excitation wavelengths. While this allows for independent determination of the in-plane thermal diffusivity, it requires data with at least two different angles. In addition, if both data sets contain only weak components due to heat flow parallel to the surface of the film, expected accuracies are low. On the other hand, with weakly absorbed excitation pulses, heat is deposited uniformly through the thickness of the film. For the case of unsupported films, this minimizes effects of out-of-plane thermal transport on the raw data itself, and allows for considerable simplification of the analysis. In fact, off-resonant excitation reduces the dimensionality of the heat flow problem and allows for extraction of thermal diffusivities with simple linear regression fitting algorithms applied to data from a single excitation wavelength. Of course, information concerning thermal transport through the plane of the film is lost. However, determination of the through-plane thermal diffusion rate from ISTS experiments with

strongly absorbed excitation pulses is facilitated once the in-plane thermal diffusivity is determined with off-resonant excitation wavelengths.

3 Data Analysis and Results

3.1 Acoustic Properties

In previous work [2], ISTS measurements were used to evaluate film acoustic parameters. To determine the elastic (or loss) moduli, the mode phase velocity (or damping velocity defined as damping rate divided by wavevector) dispersion was experimentally mapped out and fit to calculation. We followed a similar procedure with data collected in this study. The result is a significantly more accurate characterization of the intrinsic longitudinal and transverse velocities of the films.

In Fig. 8 we present data and fits for each of the six samples. These figures show data from the previous study using UV excitation pulses (open circles) and data taken from the present set of experiments using green excitation pulses (open squares). The UV data are confined to the lowest-order Lamb mode, which is antisymmetric. As expected, data from excitation with green pulses arise exclusively from symmetric Lamb modes. Although the green data are dominated by the second lowest-order Lamb mode, in the thicker samples we are also able to monitor higher order symmetric Lamb modes. We believe that this is a result of the increased interaction length for the excitation pulses. Finally, we note that in the $qd = \pi$ region there is a scarcity of data from the second lowest-order mode. This is most clearly observable in data from the 3.18, 4.40 and 5.29 μm samples. Although this behavior is consistent with theoretical arguments given in Sect. 2.1, it is difficult in practice to precisely locate the qd position at which zero excitation efficiency obtains since the excitation efficiency decreases smoothly to zero on the high and low sides of $qd = \pi$. For example, in the 8.46 μm sample where signal levels were higher than in the other samples, the second lowest mode was visible in data from all angles. The measured amplitude of this mode did however display a local

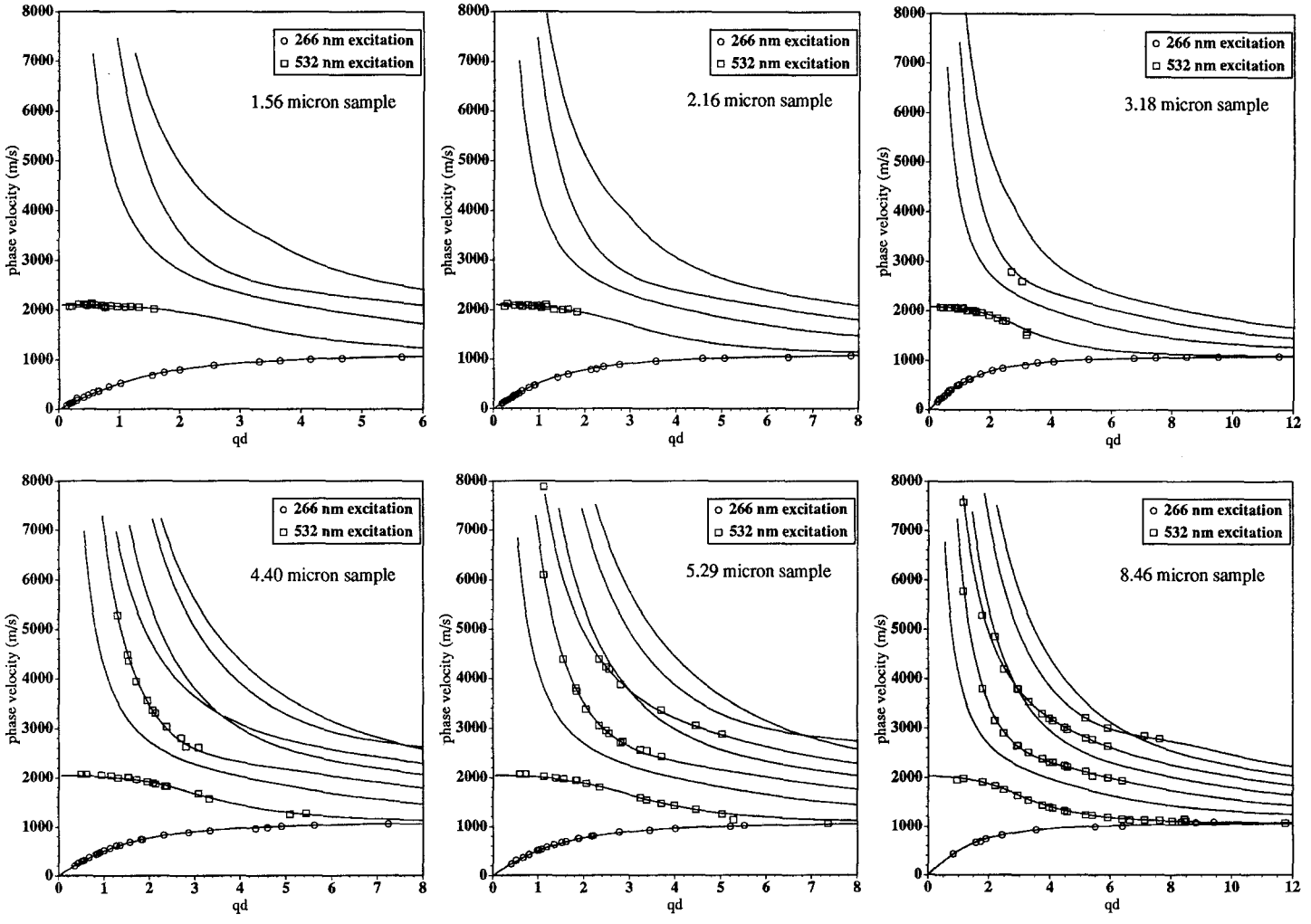

Fig. 8. Data from 266 nm (*open circles*) and 532 nm (*open squares*) excitation and best-fit calculations (*solid lines*) for a series of unsupported PI2555 polyimide films. The elastic acoustic moduli were determined through a nonlinear least-squares fit of an isotropic theoretical model to the 266 nm and 532 nm ISTS data. Agreement between theory and experiment in all cases is excellent. We also see experimental confirmation of the claim that green excitation pulses set up a symmetric driving force which only excites symmetric modes

Table 2. Summary of elastic properties of polyimide thin films as determined from measured acoustic waveguide phase velocities using data from UV and green excitation experiments

Sample thickness [μm]	Transverse velocity [m/s]	Longitudinal velocity [m/s]	Young's modulus [GPa]	Poisson's ratio
1.56	1191 ± 12	2543 ± 120	5.6 ± 0.2	0.36 ± 0.01
2.16	1167 ± 13	2683 ± 130	5.5 ± 0.2	0.38 ± 0.01
3.18	1152 ± 6	2715 ± 50	5.35 ± 0.07	0.390 ± 0.003
4.40	1161 ± 5	2467 ± 40	5.31 ± 0.06	0.358 ± 0.004
5.29	1139 ± 5	2597 ± 40	5.19 ± 0.06	0.381 ± 0.003
8.46	1126 ± 4	2570 ± 40	5.08 ± 0.05	0.382 ± 0.003

minimum in the $qd \approx \pi$ region. The apparent $\approx 10\%$ discrepancy between the predicted zero excitation efficiency qd value and the observed one is not completely understood at this time. It could be due to nonidealities not included in the theoretical description. Film anisotropy is a likely possibility, but other effects such as those of the air surrounding the film, of microscopic surface roughness, and of depth dependent elastic moduli cannot be ruled out.

The film acoustic properties determined from this work are given in Table 2. These values result from fitting the UV and green excitation data simultaneously. The uncertainties were determined from an application of the upper 90% probability point of the F distribution [2, 17]. All parameters presented in Table 2 are consistent with those determined from fitting only data resulting from excitation with UV pulses (except for the longitudinal velocity of the 4.40 μm sample which is nevertheless very close) and in every case the uncertainties determined from this study are significantly smaller than those determined using only the UV data. Young's moduli and Poisson's ratios were calculated from these best fit velocities and a density of 1450 kg/m^3 [20]. The results along with error bars are presented with the acoustic velocities in Table 2.

3.2 Thermal Properties

Reduction of the thermal diffusion data from these off-resonant excitation experiments is trivial and relies only on theoretical results for thermal diffusion in bulk samples. It is easy to show [11, 18] that if only thermal diffusion from grating peaks to grating nulls is considered, decay of the diffracted intensity should obey the relation

$$I(t) \propto \exp\left(\frac{-2q^2\kappa t}{\rho c}\right) = \exp(-2q^2 D_T t), \tag{7}$$

where $I(t)$ is the diffracted intensity, q is the wavevector magnitude given in (1), ρ is the density, C is the heat capacity per unit mass at constant strain, and κ is the thermal conductivity. D_T is known as the thermal diffusivity. For excitation angles greater than 1.30 degrees, the signal decay is single-exponential as expected from (7). At smaller angles, deviation from this behavior was observed. We suspect that this is due either to heat flow from film to air which becomes non-negligible as the grating wavelength increases, or to a heterodyning of signal light with scattered light which becomes difficult to separate from diffracted light at small angles. Because of this, data collected at small angles (< 1.30 degrees) were not used for in-plane thermal diffusivity determination. Finally, we note that the thermal decay rates (in contrast to the acoustic

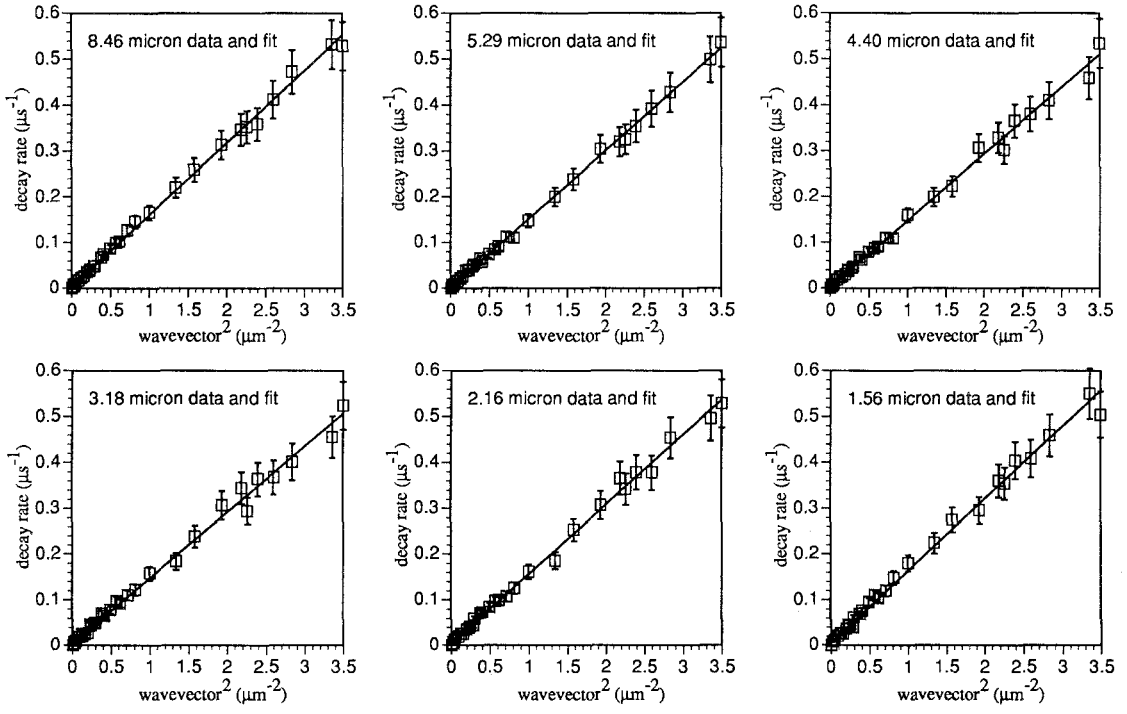

Fig. 9. Measured thermal decay rates (*symbols*) and best-fit calculations (*lines*) for a series of unsupported PI2555 polyimide films of various thicknesses. Within experimental uncertainties, the decay rates are linear in the square of the excitation wavevector and have a zero intercept. The fitted slopes yield the in-plane thermal diffusivities

Table 3. Summary of in-plane thermal diffusivities of thin polyimide films as determined from measured ISTS thermal decay rates

Sample thickness [μm]	In-plane thermal diffusivity [$\mu m^2/\mu s$]
1.56	0.077 ± 0.002
2.16	0.075 ± 0.002
3.18	0.071 ± 0.002
4.40	0.072 ± 0.002
5.29	0.074 ± 0.002
8.46	0.078 ± 0.002

frequencies) varied from spot to spot on the samples by as much as 15% and typically by 5–7%. For analysis we used the average of thermal decay rates measured at two different spots at each excitation wavelength.

Through linear least-squares analysis of the logarithm of the measured decays (see Fig. 4B), we can determine the argument of the exponential given in (7). In Fig. 9 we plot the fitted decay rates as a function of the square of the wavevector. As expected, the data in each case are very closely described by a straight line with zero intercept. The slope of this line gives the thermal diffusivity. Results for the six polymer films are given in Table 3 along with uncertainties determined from a 90% confidence level cumulative t distribution statistic [19].

4 Discussion

In Figs. 10 and 11 we present results for elastic and thermal properties of the polyimide films as functions of thickness. In the previous work, data suggested slightly decreasing stiffness with increasing thickness although the trends were within error bars. The acoustic parameters from this study have smaller error bars and enable a more rigorous test of possible thickness dependences of film properties. From Fig. 10A the transverse velocity decreases slightly with increasing thickness which is consistent with what we found previously. On the other hand, from Fig. 10B no systematic thickness dependence to the longitudinal velocity is evident. We have described possible explanations to account for the slight thickness dependence of the elastic fitting parameters [2].

In Fig. 11 the thermal diffusivities measured in this study and a value for the out-of-plane thermal diffusivity in thick (≈100 μm) PI2555 films measured by Dupont [20] are displayed. Since the Dupont value corresponds to an out-of-plane measurement while our measurements only concern in-plane diffusion, and since samples of significantly different thickness were used, there is no reason to expect the results to coincide precisely. We find that our measurement and Dupont's differ by about 20%. Finally, from Fig. 11 some sample to sample variation in the thermal diffusivity is evident. Without more samples, it is difficult to say whether the variation is systematic and thickness dependent or random.

As mentioned at the outset, use of off-resonant excitation reduces the effort needed to determine the acoustic and the thermal properties of the film because it allows for

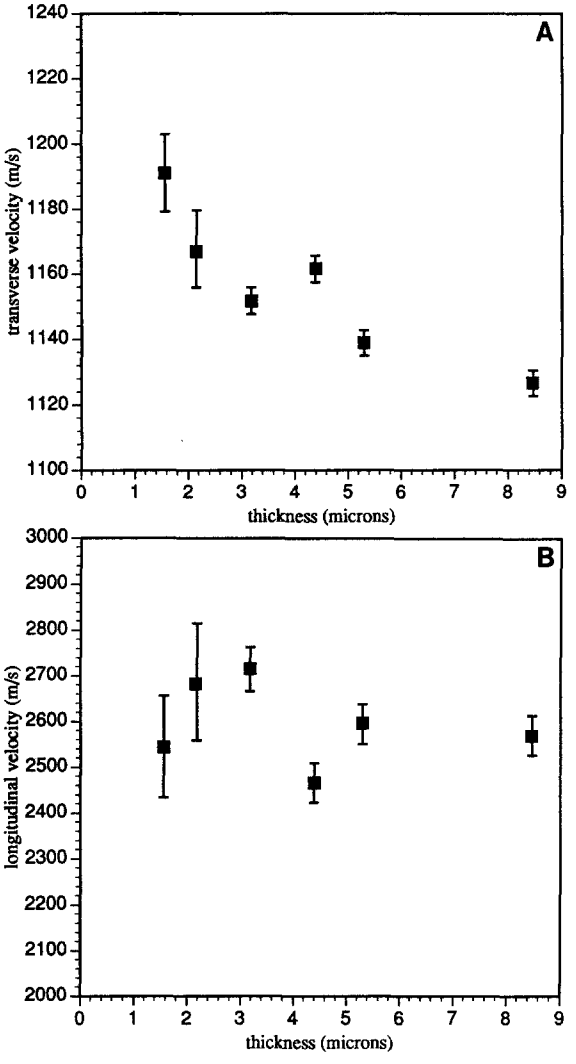

Fig. 10A, B. Experimentally determined transverse (**A**) and longitudinal (**B**) film velocities as a function of thickness. A weak trend toward smaller transverse velocities with increased thickness is suggested. No such trend in the longitudinal velocity is discernable

observation of the second lowest-order mode and because it reduces the dimensionality of the heat flow problem. The characterization problem is further simplified in the thicker samples where multimode acoustic propagation is measurable. Because of this, it is possible to completely characterize the elastic properties of the thicker films with a single laser shot at a single excitation angle. To demonstrate this, we fit the acoustic and thermal data from the 8.46 μm film at an excitation wavevector of 0.47 μm^{-1} and 0.70 μm^{-1}. For the former, there are three measured acoustic waveguide velocities from which the longitudinal and transverse velocities are determined, whereas for the latter there are four. For the first case, the fitted longitudinal velocity is 2593 ± 100 m/s and the transverse velocity is 1124 ± 50 m/s. For the second case, the longitudinal velocity is 2610 ± 70 m/s and the transverse velocity is 1129 ± 20 m/s. These fitted parameters are consistent both with those determined from fitting all data at all wavevectors

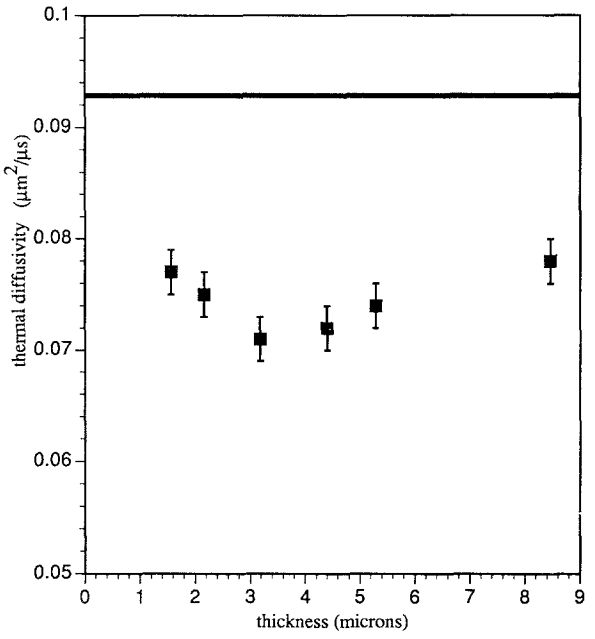

Fig. 11. Experimentally determined in-plane thermal diffusivity as a function of film thickness. No systematic thickness dependence is evident. The heavy *solid line* indicates an out-of-plane thermal diffusivity measured in a much thicker film by Dupont. Although there is no reason to expect precise agreement between values measured here and those of Dupont, the results are within 20%

and from fitting only UV excitation data at all wavevectors. While the error bars for these single angle determined velocities are larger than those of Table 2, they are comparable to those determined using UV excitation data at 17 angles. These effects are illustrated in Fig. 12. Figure 12 A shows a contour plot of the error surface for the UV excited data alone, Fig. 12 B shows a similar plot for green excited data at 0.70 μm^{-1}, and Fig. 12 C is for all of the UV and green data. These figures clearly show that while the transverse velocity is well determined in each case, the uncertainty in the longitudinal velocity is dramatically decreased when other than the lowest-order mode is used.

As discussed before, the advantage of off-resonant excitation for film thermal diffusion evaluation is that the in-plane thermal diffusivity can be determined with linear regression algorithms applied to data at a single angle. To demonstrate this, we fit thermal data from the 8.46 μm sample at the two wavevectors used in the single angle acoustic moduli evaluation described in the previous paragraph. The results are 0.087 ± 0.015 $\mu m^2/\mu s$ at 0.47 μm^{-1} and 0.088 ± 0.015 $\mu m^2/\mu s$ at 0.70 μm^{-1}. As with the acoustic moduli, these diffusivities are consistent with those arrived at by using all of the data. Again, while the error bars are slightly larger, the diffusivities are well determined at a single excitation angle. This leads us to the conclusion that, since data at each of these excitation angles are collectable in a single shot, it is possible to completely characterize the in-plane thermo-mechanical properties of an isotropic polymer film with ISTS in a single laser shot.

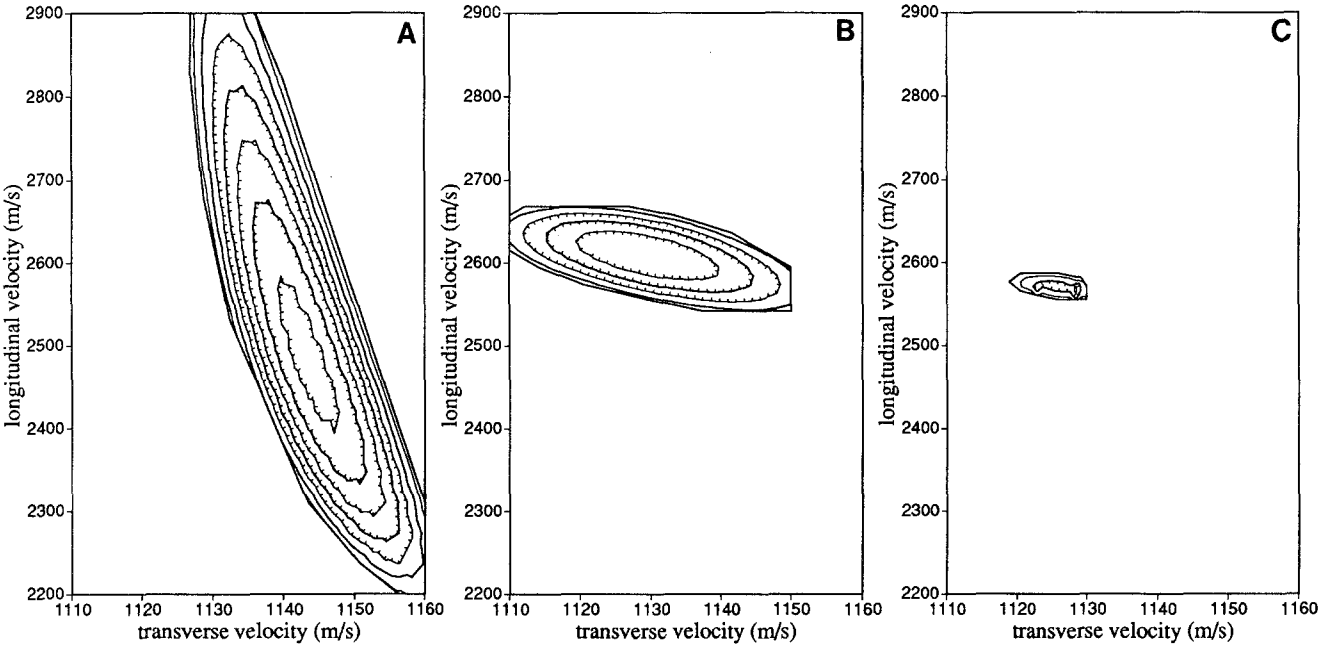

Fig. 12A–C. Contour plots of the sum of squares error surfaces for UV excitation data from 17 different angles (**A**), green excitation data from a single angle (**B**), and UV and green excitation data from ~30 different angles (**C**). The sum of squares errors is plotted on the *z*-axis and the fitting parameters, the longitudinal and transverse velocities, are plotted on the *x*- and *y*-axes. Note that the *x*- and *y*-axes have the same scale and range in each of the three parts. The errors are plotted up to a value near that which is first considered significant according to the upper 90% probability point *F* distribution. From these figures it is seen that although the transverse velocity is well determined in each case, the longitudinal velocity is only determined accurately when modes other than the lowest one are monitored

5 Conclusions

We have shown that with off-resonant excitation we can selectively excite symmetric Lamb modes in thin unsupported polymer films. Data analysis shows how the dispersion of these modes provides a means through which intrinsic film longitudinal and transverse velocities can be determined with a high degree of accuracy.

We have also used the data to determine the in-plane thermal diffusivity. With weakly absorbed excitation pulses, the dimensionality of the heat conduction problem is reduced, and data analysis is greatly simplified. Our results are within 20% of independent measurements [20].

Acknowledgements. We wish to thank D. Volfson and F. Trusell for assistance with sample preparation. This work was supported by NSF Grant No. DMR-9002279, by the Donors of the Petroleum Research Fund, administered by the American Chemical Society, and by the Electronics Packaging Program at M.I.T.. J.A.R. acknowledges the support of a NSF doctoral fellowship.

References

1. A.R. Duggal, J.A. Rogers, K.A. Nelson: J. Appl. Phys. **72**, 2823 (1992)
   A.R. Duggal, J.A. Rogers, K.A. Nelson, M. Rothschild: Appl. Phys. Lett. **60**, 692 (1992)
   J.A. Rogers: M.S. Thesis, Massachusetts Institute of Technology (1992)
2. J.A. Rogers, K.A. Nelson: J. Appl. Phys. **75**, 1 (1994)
3. H.J. Eichler, P. Günter, D.W. Pohl: *Laser-Induced Dynamic Gratings*, Springer Ser. Opt. Sci., Vol. 50 (Springer, Berlin, Heidelberg 1986)
4. K.A. Nelson, M.D. Fayer: J. Chem. Phys. **72**, 5202 (1980)
   K.A. Nelson, D.R. Lutz, M.D. Fayer, L. Madison: Phys. Rev. B **24**, 3261 (1981)
5. J.S. Meth, C.D. Marshall, M.D. Fayer: J. Appl. Phys. **67**, 3362 (1990)
   J.S. Meth, C.D. Marshall, M.D. Fayer: Chem. Phys. Lett. **162**, 306 (1989)
6. P. Korpiun, B. Merte, G. Fritsch, R. Tilgner, E. Luscher: Colloid Polym. Sci. **261**, 312 (1983)
7. P. Cielo, L.A. Utracki, M. Lamontagne: Cdn. J. Phys. **64**, 1172 (1986)
8. J. Rantala, J. Jaarinen, P.K. Kuo: Appl. Phys. A **55**, 586 (1992)
9. N. Tsutsumi, T. Takizawa, T. Kiyatsukuri: Polymer **31**, 1925 (1990)
   N. Tsutsumi, N. Takeuchi, T. Kiyatsukuri: J. Polym. Sci. B **29**, 1085 (1991)
10. G. Busse, P. Eyerer: Appl. Phys. Lett. **43**, 355 (1983)
11. C.D. Marshall, I.M. Fishman, M.D. Fayer: Phys. Rev. B **43**, 2696 (1991)
    C.D. Marshall, I.M. Fishman, R.C. Dorfman, C.B. Eom, M.D. Fayer: Phys. Rev. B **45**, 10009 (1992)
12. J.Y. Pan: Ph.D. Thesis, Massachusetts Institute of Technology (1991)
13. H. Robbins, B. Schwartz: J. Electrochem. Soc. **107**(2), 108 (1960)
14. F. Maseeh, M.A. Schmidt, M.G. Allen, S.D. Senturia: Calibrated measurements of elastic limit, modulus and the residual stress of thin films using micromachined suspended structures, in IEEE Solid-State Sensor and Actuator Workshop (1988) p. 23
15. F. Maseeh, S.D. Senturia: In *Polyimides: Materials, Chemistry, and Characterization*, ed. by C. Feger, M.M. Khojasteh, J.E. McGrath (Elsevier Amsterdam 1989) pp. 575–584
16. W. Nowacki: *Themoelasticity* (Pergamon, New York 1986)
17. E.M.L. Beale: J. R. Stat. Soc. B **22**, 41 (1960)
    E.S. Pearson, H.O. Harley: *Biometrika Tables for Statisticians* (Cambridge Univ. Press, Cambridge 1970)
18. A.R. Duggal, K.A. Nelson: J. Chem. Phys. **94**, 7677 (1991)
19. J.W. Barnes: *Statistical Analysis for Engineers* (Prentice Hall, Englewood Cliffs 1988)
20. Technical Data Sheet, DuPont Co., Semiconductor Materials, Wilmington, DE